Wedge indentation of elastoplastic solids - from single indentation to interaction between indenters

Yvan Marthouret, Tony Zaouter, Florent Ledrappier, Guillaume Kermouche

Wedge indentation of elastoplastic solids – from single indentation to interaction between indenters

Yvan Marthouret[1,2], Tony Zaouter[2], Florent Ledrappier[3], and Guillaume Kermouche[1]

[1] Mines Saint-Étienne, CNRS UMR 5307 LGF, Centre SMS, Saint-Étienne F42023, France
[2] CEA, DES, ISEC, DE2D, SEAD, Laboratoire d'Étanchéité Maestral, Univ. Montpellier, Marcoule, France
[3] TECHNETICS Group France, Laboratoire d'Étanchéité Maestral CEA–Technetics, Pierrelatte, France

Performance of metallic seals used between face-turned surfaces is related to their abilities to flow plastically in order to fill up cavities between wedge-shaped asperities. Multiple wedges indentation is therefore a simple way to investigate what happens at such a seal–flange interface. In this paper, finite element analyses of single and multiple wedges indentations are conducted. A particular attention is paid to the effects of hardening parameters on the resulting hardness. First, it is observed that single wedge indentation hardness can be well-approximated by the adaptation of analytic models initially developed for cone indentation problems. Second, it is shown that interaction between indentation-strain field during multiple wedges indentation starts once the bearing ratio is about 25%. It leads to a significant mean contact pressure increase, which is strongly dependent upon the strain hardening exponent. Eventually, for a bearing ratio higher than 75%, a plastic locking stage occurs, which leads to a fast increase of the mean contact pressure. Practical applications of this work to indentation and sealing research fields are discussed.

Keywords wedge, indentation, FEM, roughness interaction, metallic seals

1 Introduction

High-performance sealing applications rely on the use of entirely metallic seals. Their efficiency is directly related to the ability for the soft metallic outer liner of the seal to plastically flow in and around the topographical defects of the facing rigid rough surfaces, to reduce the leakage paths at the seal–flange interface (Pérez-Ràfols et al. 2016). In many applications, the flat surface of the rigid flanges are obtained through face turning (Robbe-Valloire et al. 2008). With such manufacturing process, the resulting surface possesses a characteristic spiral-grooved texture (see Fig. 1). The resulting topography can be approximated by arrays of wedges (Fig. 1), the dimensions of which being directly related to the process parameters (feeding rate, cutting depth) and tool geometry (tool tip radius) as presented in Dumas et al. (2021). Therefore, modelling of multiple wedges indentation can be of prime importance to better understand the sealing mechanism of a rough rigid flange by a metallic gasket. The problem of sealing can thus be viewed as a matter of describing the evolution of the gap at the seal–flange interface (at the roughness scale) as a function of the applied normal load on the contact. This latter depends on wedge indentation-induced contact pressure, that is the wedge indentation hardness.

Sharp indentation of elastoplastic solids has been widely investigated during the last three decades, mostly because of the huge interest brought by the use of nanoindentation testing to characterize mechanical properties of materials at a very small scale (Oliver et al. 1992; Cheng et al. 2004). However most of the developments were devoted to conical or pyramidal indentation tests with only a few articles related to wedge indentation. Since wedge indenters are self-similar when the contact is made along the apex of the wedge, the principle of geometric similarity holds provided that the indented solids are semi-infinite and that there is no internal length to account for (Kermouche et al. 2005). Consequently the hardness (i.e., the mean contact pressure) does not depend upon loading parameters such as the applied load or the displacement relative to the surface. The hardness is thus a function of material properties and tip geometry only, here the tip angle for wedge indentation. In the case of wedge indentation of rigid perfectly plastic solids, a direct relation can be made between the hardness and the yield stress through slip lines theory of Hill (1950). An exact solution for wedge indentation of linear isotropic elastic solids was also derived from Boussinesq's theory by Johnson (1987). Between these two cases, an approximate elastoplastic solution was derived through the concept of the representative elastic material that makes it possible to relate the hardness to the yield stress accounting for materials elasticity (Kermouche et al. 2005). Surprisingly, methods based on expanding cavity analogies (Gao et al. 2006; Feng et al. 2007) were not used to model wedge indentation, although their extension to this framework seems straightforward. Consequently there is still a need nowadays to investigate which models lead to the best prediction of hardness of elastoplastic solids when indented by a wedge.

Single wedge indentation corresponds to the first stage of sealing, when the distance between two successive peaks is significantly larger than the contact length of a single peak. For a given contact length,

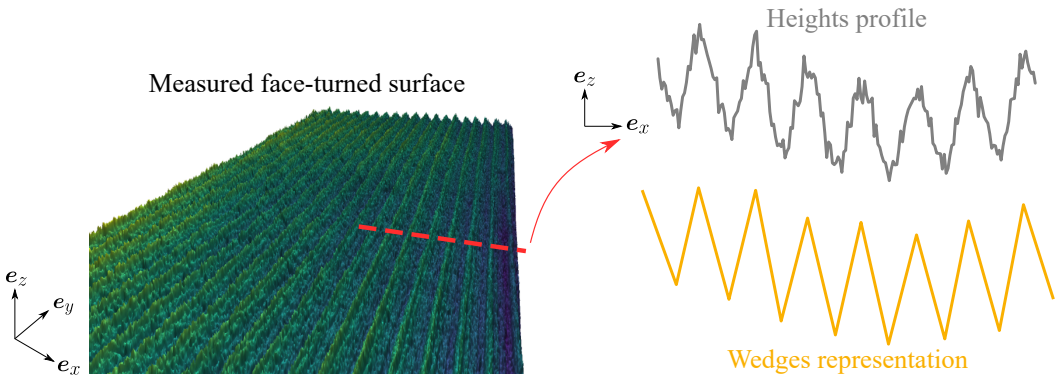

Figure 1: Topography of a measured face-turned rough surface. The representation of a radial profile by an array of wedge indenters is shown on the right.

the indentation-induced strain fields of the two successive peaks start to interact, which violates the principle of geometric similarity (Tabor 1951; Cheng et al. 2004). Therefore the hardness becomes a function of the ratio of the contact length and the distance between the peaks. Only a few papers (Meguid, Collins, et al. 1977; Salikhyanov 2019) have dealt with such a problem since it requires an incremental approach to derive an analytical solution through the slip lines theory. It is shown that two stages occur after the single wedge indentation stage. The first stage is the interaction stage that corresponds to the interaction between the two neighbouring indentation strain fields. Within this stage, the hardness increases. This stage ends when the interaction between the two indentation strain fields result in a global plastic locking. At this point the sealing cannot be improved anymore but is not terminated. To enter the last stage of sealing, it is required that the plastic strain field interacts with some interfaces or boundary conditions that forces the materials to flow up again. Eventually the remaining gap is filled with the sealing materials and the sealing is over. There is clearly a need to investigate in a deeper way how to describe these last two stages.

This article is organized as follows. First, we describe two single wedge hardness models developed for Hollomon-based strain hardening elastoplastic solids. The results are compared to Finite Element calculations to evidence the limitation of these two models. Then, we propose to investigate the interactions between two neighbouring wedges using a Finite Element Analysis. Results are given in terms of apparent hardness and compared to single wedge hardness. A particular attention is paid to the identification of different interaction regimes from the single wedge indentation one to the final sealing stage. Finally, conclusions and perspectives of this study are given.

2 Theoretical framework

2.1 Single wedge indentation models

As a versatile and easy-to-measure mechanical property, hardness is widely studied in the literature. Several well-known models predict its value for rigid perfectly plastic solids through the slip lines method of Hill (1950) or the empirical method of Tabor (1996). They lead to the conclusion that hardness is a measure of the yield stress of a material through Eq. (1) where $\mathcal{H}_{mat}$ is the material hardness, σ_Y is the yield stress of the material and β the tip-to-surface contact angle

$$\frac{\mathcal{H}_{mat}}{\sigma_Y} = f(\beta). \tag{1}$$

However, real engineering materials exhibit non negligible elasticity and strain hardening so that models developed for rigid perfectly plastic solids can lead to strong discrepancies. In such case, the hardness is typically formulated as a function of supplementary material parameters as

$$\frac{\mathcal{H}_{mat}}{\sigma_Y} = f\left(\beta, \frac{E}{\sigma_Y}, n\right), \tag{2}$$

with E the Young modulus and n the hardening exponent. In this work, we propose to compare two analytical models, the Expanding Cylindrical Cavity model (ECC) from Johnson (1987); Gao et al. (2006) and the Representative Elastic Material model (REM) derived from Tabor (1951). These two models take strain hardening into account and are briefly introduced in the following sections.

2.1.1 The Expanding Cylindrical Cavity model (ECC)

For the ECC model, the stress and strain fields under the apex of the wedge are idealized as the expansion of a cylindrical cavity subject to hydrostatic pressure. Johnson (1970) first offered this modelling for

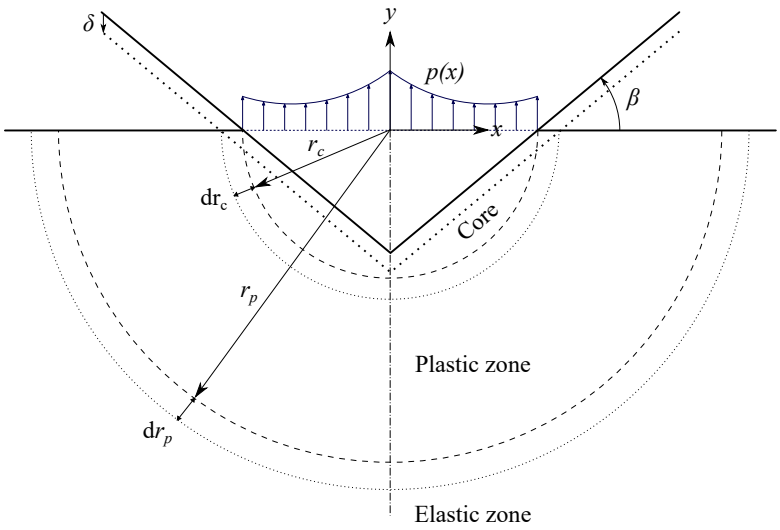

Figure 2: Schematic representation of the cylindrical cavity expansion under a wedge indenter.

conical and wedge indenters in elastic perfectly plastic materials. However, it does not take into account the strain hardening of real materials.

$$\sigma = \sigma_Y^{1-n} \, (E\varepsilon)^n \tag{3}$$

Later, Gao (2003); Gao et al. (2006) extended the use of such model to obtain an analytical formulation for conical and spherical hardness for a elastoplastic material following Hollomon's power-law hardening (eq. 3) with σ the equivalent stress, σ_Y the yield stress, E the Young modulus, n the hardening exponent and ε the total equivalent strain. Fig. 2 gives a representation of the plane strain cylindrical expansion of cavity, to be applied to determine the hardness in single wedge indentation of elastoplastic solids. A summary of the model is given here for general comprehension. Considering a semi-infinite half space, indentation creates a dead volume which does not deform, joined together with the tip. This core volume is considered as a cylindrical cavity which expands itself in the material under a hydrostatic pressure linked to the mean pressure under the tip (i.e., material hardness). From the classical solution of an elastoplastic cylinder subject to internal pressure, stress and displacement fields can be derived (Gao 2003). It yields an elastic zone ($r > r_p$) where the material remains elastic, and a plastic zone ($r_c > r > r_p$) where material undergoes plastic deformation. The radius of the plastic zone r_p is determined by the internal pressure and the radius of the cavity, or core, r_c. As shown on Fig. 2, an increment of indentation δ induces an expansion of the core. The volume of material being conserved, this expansion is equivalent to the volume of material displaced by the wedge which depends of the contact angle β. The radial displacement being known for the cylinder expansion, the quantities r_p and r_c can be related with one another and further with the total displaced volume. Hence, the internal pressure can be expressed, depending only on the material characteristics and the contact angle of the wedge.

According to our assumption, the internal pressure should be equal to the hardness of the material $\mathcal{H}_{mat}$. However, it is known that the model based on Johnson (1970) underestimates the hardness. To this end, Studman et al. (1977) and Gao et al. (2006) propose a correction to the expression of this internal pressure based on the stress discontinuity occurring at r_c. Following a similar correction for the case of wedge indentation, the modified ECC model gives a corrected hardness $\mathcal{H}_{mat}$ in Eq. (4), showing a dependency to the yield stress σ_Y, the strain hardening coefficient n and Young's modulus E arising from Hollomon's and Hooke's laws. According to principle of geometrical similarity, the only geometrical parameter is the contact angle β

$$\mathcal{H}_{mat} = \frac{\sigma_Y}{\sqrt{3}} \left\{ 1 - \frac{1}{n} + \left(\frac{\sqrt{3}}{2} + \frac{1}{n} \right) \left(\frac{2}{\pi\sqrt{3}} \frac{E \tan\beta}{\sigma_Y} \right)^n \right\}. \tag{4}$$

2.1.2 The Representative Elastic Material model (REM)

This model has been extensively described in Kermouche et al. (2005) and thus only the main features are given hereafter. To describe the indentation of materials and based on empirical considerations, Tabor (1951) proposed to define a representative stress σ_r and a representative strain ε_r, characteristic of the process under concern. The REM model defines a representative elastic material whose stress–strain curve passes through the $(\varepsilon_r, \sigma_r)$ couple of the indented material. The Young modulus of the representative material is thus simply defined as $E_r = \sigma_r/\varepsilon_r$. The representative strain can be split into a an elastic and a

plastic part as $\varepsilon_r = \varepsilon_r^e + \varepsilon_r^p$, with the elastic part being given by $\varepsilon_r^e = \sigma_r/E$. Following the suggestion of Tabor, the representative plastic strain ε_r^p can be chosen as proportional to the tangent of the contact angle β as $\varepsilon_r^p = \zeta \tan\beta$. Note that when the contact angle is "small", only elastic strain may take place. Hence, a threshold contact angle β_0 has to be considered. The hardness (mean contact pressure) of the representative elastic material can be formally derived using the linear elastic contact theory for a wedge as (Sneddon 1965)

$$p_m = \frac{1}{2}\frac{E_r}{1-\nu_r^2}\tan\beta, \tag{5}$$

where ν_r is the representative Poisson coefficient, often taken as 0.5. Then assuming that the coefficient of proportionality between the hardness and the representative stress is the same for the representative elastic material and the indented material, the hardness of the latter is given by

$$\mathcal{H}_{mat} = p_m = \frac{1}{2(1-\nu_r^2)}\frac{\zeta\sigma_r\tan\beta}{\zeta\tan\beta + (1-\zeta)\frac{\sigma_r}{E}}, \tag{6}$$

where ζ is a function of the representative Poisson's ratio and the contact angle. In Eq. (6), Young's modulus E and contact angle β are used explicitly. However, the hardening coefficient n and yield stress σ_Y are implicitly found in the calculation of the representative stress σ_r from the representative strain ε_r (see Kermouche et al. (2005) for more details).

2.2 Multiple wedges indentation

To avoid artefacts related to interactions between neighbouring indents, the usual rule consists in separating two successive indents with a distance about twenty times that of the penetration depth. This empirical rule is actually based on the dimension of the plastic zone beneath an indent. This zone is often assumed as spherical for pyramidal indentation, cylindrical for wedge indentation, with a radius about three times the contact radius. For Berkovich and Vickers tips ($\beta \approx 20°$), the contact radius is about three times the penetration depth. This is the reason why the plastic zone length is often assumed as ten times the penetration depth, which leads to define a distance between two neighboring indents about twenty times the penetration depth to avoid interaction artefacts. For a Cube corner tip ($\beta \approx 45°$), this distance should be significantly smaller, but for asperity angles typically found in sealing ($\beta \lesssim 10°$) it should be much larger. Hence the validity range of single wedge indentation appears to be very limited to investigate a sealing process.

Application of slip lines theory to interacting wedges were recently proposed by Salikhyanov (2019). It was developed for contact cold welding of metallic plates which is somewhat close to the sealing process. The substrate is a rigid perfectly plastic infinite half-space but such a theory can be extended to finite media (Hill 1950a). The main drawback is that a perfectly plastic material does not deform elastically neither harden. Hence it cannot be expected to transpose the derived results to a real case in a quantitative manner. Such an approach was successfully used for single wedge indentation (Hill 1950b; Johnson 1987) and allows to highlight some interesting features, such as the relation between hardness and yield stress, the pile-up geometry or the wedge angle effect. From this point of view the work of Salikhyanov (2019) pointed out some interesting features in the framework of the interaction of two neighboring wedges through the interaction of two wedge indentation slip lines fields.

As expected, the self-similarity is lost when the two slip-line fields start interacting and the hardnesss (mean contact pressure) starts increasing. This interaction creates an entirely new slip-line field, as shown in Salikhyanov 2019, which is a combination of the previous slip-lines with a growing interaction area in the center of the groove. It effectively transforms plastic flows under both wedges, from known Hill solution's pile-up to a uniform rise (wedge symmetry) of the surface in the groove. With symmetric wedges, previous pile-up is gradually recovered by the rising surface while the interaction area grows progressively replacing the usual slip-line fields. A plastic locking stage is reached as the two slip-line fields fully recover, it is described as the third stage of Salikhyanov 2019. At this point, the surface between wedges is perfectly flat (by symmetry) and the unified slip-line field does not enable anymore material flow. Hence, the closing of the groove is stopped. This state is mostly caused by the symmetry of recovering fields and can not be resolved in the semi-infinite case treated by Salikhyanov 2019. However, a third interaction (through the presence of the substrate boundary or another asperity) in a finite space framework as shown in Hill 1950a can force the materials to flow up again. ~~As expected, the self-similarity is lost when the two slip line fields start interacting. The hardness (mean contact pressure) starts increasing up to the plastic locking process that happens when the two slip line fields fully recover. The last stage of sealing can occur only if the resulting slip line field interacts with another one (through the presence of the substrate boundary or another asperity) that forces the materials to flow up again.~~ Consequently the contact between the wedge-shaped asperities and the material can be described through an apparent hardness $\mathcal{H}$, which is *a priori* higher than the single wedge material hardness $\mathcal{H}_{mat}$. This apparent

hardness is a function of geometrical parameters (contact angle β, distance between wedges W, penetration depth δ and projected contact area L_c) as well as elastoplastic material parameter as

$$\frac{\mathcal{H}}{\sigma_Y} = f\left(\beta, \frac{\delta}{L_c}, \frac{W}{L_c}, \frac{E}{\sigma_Y}, n\right). \tag{7}$$

3 Numerical framework and simulations

The Finite Element Method (FEM) has been widely used in the past decades to explore the mechanical response of materials under indentation loading and to check analytical models derived for that purpose (Cheng et al. 2004; Poon et al. 2008). Hereafter FEM is used to compare the two analytical models derived for single wedge indentation. Then a FEM investigation of interacting wedges is proposed to explore how the apparent hardness is affected by material properties and geometrical parameters. In this section, the two single and multiple wedge indentation FE models are described in details.

3.1 Single wedge indentation

Calculations have been performed with the commercial FEM code ABAQUS® using 2D plane strain elements to model wedge indentation, and using a large displacement–large strain option (updated Lagrangian formulation, logarithmic strain). ~~The mesh is especially refined near the contact zone, but is also sufficiently wide to approximate a semi-infinite solid (see Fig. 3).~~ The mesh is refined enough in the contact zone to prevent mesh size effects. It then becomes progressively coarser farther away from the contact zone, and a wide bulk is used to approximate a semi-infinite solid (see Fig. 3). A mesh convergence study has been performed and is presented in appendix A. For a good representation of the contact geometry, the width of the elements has been determined so as to have at least 37-66 nodes in contact for the deepest penetration. The whole mesh contains about 4285 elements and 4374 nodes. The contact between the indenter and the workpiece is assumed to be frictionless and loading is monitored by prescribing a vertical quasi-static displacement of the indenter into the surface. Furthermore, the indenter is assumed to be perfectly rigid. The plastic flow is described by a von Mises yield criterion coupled to isotropic strain hardening. The stress–strain curves follows Hollomon's power-law hardening (eq. 3) described by three parameters, namely the initial yield stress σ_Y, the strain hardening exponent n and the Young modulus E. This very simple elastic-plastic behaviour can be easily implemented in any FE software such as ABAQUS® by tabulating the yield stress as a function of the cumulated plastic strain, i.e. the unixaial plastic strain during a monotonous uniaxial tensile test. For that purpose, for a given set of parameters, the plastic strain is computed from uniaxial stress σ and uniaxial strain ε by:

$$\varepsilon_p = \varepsilon - \frac{\sigma(\varepsilon)}{E} \tag{8}$$

where $\varepsilon = \varepsilon_e + \varepsilon_p$, $\varepsilon_e = \frac{\sigma(\varepsilon)}{E}$ being the uniaxial elastic strain. For a given set of parameters, the uniaxial stress is given by the Hollomon law from equation 3. As shown in Cheng et al. (2004), the effects of the contact angle β and the Young modulus E on the hardness can be deduced from dimensional analysis. As a consequence, it is chosen in the present work to mostly investigate the effects of Hollomon's hardening parameters σ_Y and n on the resulting wedge hardness. The main advantage of such law resides in its few parameters which allow for an extensive parametric study and a simplified use in analytical developments such as ECC and REM models. However, it does not describe accurately the real behaviour of materials especially for high deformations. Young's modulus and Poisson's ratio are arbitrarily taken as those of steel ($E = 210$ GPa and $\nu = 0.3$). The value of the contact angle has been fixed to $\beta = 20°$. For this parametric, the (σ_Y, n) values are chosen from a regular "grid", with 10 MPa $\leqslant \sigma_Y \leqslant$ 500 MPa by increments of 10 MPa and $0.1 \leqslant n \leqslant 0.5$ by increments of 0.05. This leads to a total of 450 simulations populating the parametric space. Hereafter it is proposed to compare the performance of the two analytical ECC and REM models (given by Eqs. (4) and (6) respectively) in predicting the material hardness for material properties typical of those found in metallic seals materials (aluminium, copper, silver, etc.)

For each simulation, the total vertical force F and the projected contact length L_c can be computed. Note that since the problem is treated in plane strain, F is homogeneous to a force per unit depth (direction of the axis of the wedge), but simply denoted as "force" in the subsequent for simplicity. The hardness is further obtained as the mean vertical contact pressure and given by

$$\mathcal{H}_{mat} = \frac{F}{L_c}. \tag{9}$$

Single wedge indentation of semi-infinite half space satisfies the principle of geometric similarity, the hardness is computed for all computational frames and an average is performed on these frames to eliminate any discrete mesh effects.

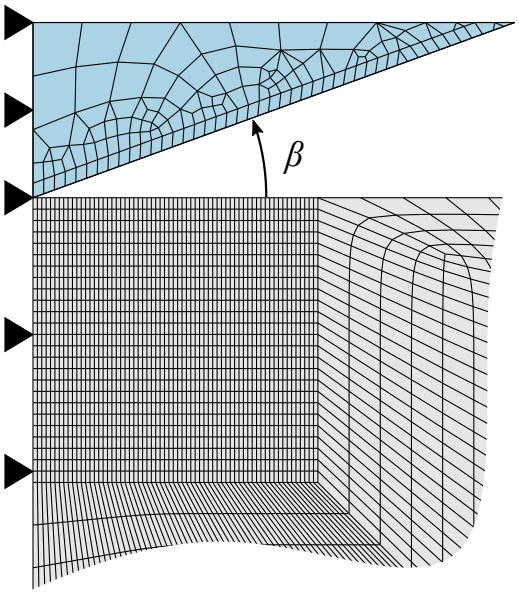

Figure 3: Single indentation FEM simulation in ABAQUS®. Partial view of the mesh of the indenter (blue) and the substrate (grey).

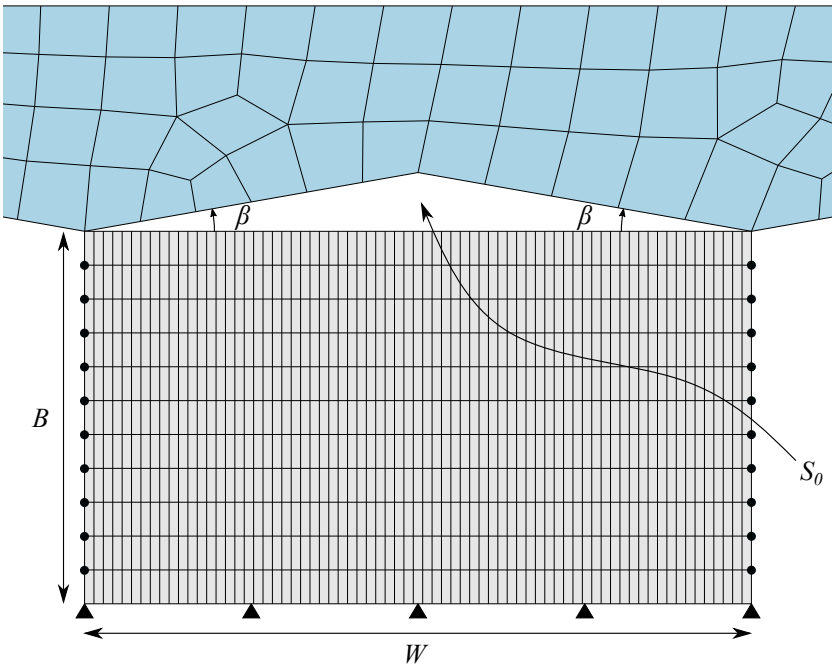

Figure 4: Scheme of the multiple wedges indentation geometry. The indenter is shown in blue and the substrate in grey. The mesh represented here is coarser than that used in the simulations for clarity.

Table 1: Values of geometrical parameters used for the FEM simulations

Geometry	β	B [mm]	W [mm]
#1	10°	1.00	0.10
#2	10°	1.00	0.50
#3	10°	0.30	0.10
#4	5°	1.00	0.35
#5	5°	1.00	0.10

3.2 Multiple wedges indentation

In the framework of sealing, interaction between rigid asperities is clearly too complex to be investigated in a purely analytical way. Hence FEM appears as a method of choice to explore such phenomena. It has already been used on one hand to deal with interacting flat punches (Meguid and Klair 1985) or to assess the validity of the slip line fields proposed by Salikhyanov (2019). In this paper, we design a geometry of multiple wedges indentation based on this latter approach (see Fig. 4). The effects of geometrical parameters that is proposed to be explored in this work are the distance between the two neighboring wedges W and the contact angle β. Periodic boundary conditions are applied on the left and right side of the model, making the so-called double indentation a multiple wedges indentation with a virtual infinity of wedge indenters. Thus the double wedge is viewed as a unit cell for the periodic problem. The bulk height B is also taken into account since it also plays a role on sealing (it can be viewed as the thickness of the sealing outer liner), in particular at the last stage of sealing. The two wedges being similar in this paper, the reader may notice that a supplementary vertical symmetry in the middle of the two indenters could have been used. This is due to the fact that the present numerical model was first designed to handle the general case of asymmetrical indenters. We chose however to focus only the results for the symmetrical case in the present paper.

Similarly to the case of single indentation, the simulations have been performed with ABAQUS® using 2D plane strain elements to model wedge indentation and using a large displacement–large strain option (updated Lagrangian formulation, logarithmic strain). The contact between the indenter and the substrate is considered frictionless and the wedge indenters perfectly rigid. The whole mesh contains about 6420 elements and 6648 nodes (see Fig. 4). A convergence study presented in appendix B justifies the use of a rather coarse mesh (ratio of element size on indenter tips distance $\approx 1\,\%$). This trade off is done to permit an extensive parametric analysis of the multiple wedges indentation which can be quite demanding in terms of computational time, especially because of contact convergence issues. The mechanical behaviour of the substrate is described through the same constitutive model than the one used for single wedge indentation (Hollomon's power-law hardening).

Hereafter it is proposed to explore the effects of Hollomon's parameters on the apparent wedge indentation hardness $\mathcal{H}$. We choose to focus on hardening parameters in the range $0.05 \leqslant n \leqslant 0.4$ and $20\,\text{MPa} \leqslant \sigma_Y \leqslant 200\,\text{MPa}$ in the simulations. Since multiple wedges indentation does not satisfy the principle of geometric similarity when wedge-induced strain fields start interacting, the hardness is computed at each computational step. The reaction force of the double wedge is taken at each increment and divided by the current projected contact area to compute the apparent hardness of the multiple wedges indentation. ~~A sliding average filter is applied to eliminate mesh-induced artificial oscillations due to the discrete evolution of the contact length.~~ As observed on Fig. 19 from the convergence study in appendix B, a coarse mesh does not change the average value and evolution of our quantities. However, the discrete evolution of the contact length produces artificial oscillations which are quite misleading. A sliding average filter is hence applied. The convergence study validates this approach with Fig. 20 comparing averaging coarse mesh hardness evolution with refined mesh one. This new instantaneous hardness is called apparent hardness, $\mathcal{H}$. The results will be interpreted through the evolution of this parameter as a function of the projected contact length. With sealing purposes in mind, it is interesting to follow the closing of the aperture. Consequently, the evolution of the current opening between bulk and indenter S (comparable to the free volume under the indenter) is monitored during the indentation process. Five indenter geometries are investigated to highlight the influence of geometrical parameters defined in Fig. 4. The five sets of parameters employed are summarized in Tab. 1.

4 Results and discussion

4.1 Single wedge indentation

The accuracy of both the ECC and the REM analytical models are assessed with the help of finite element modelling of single wedge indentation. To do so, the relative error defined in Eq. (10) is used, with $\mathcal{H}_{mat}$ the material hardness given by the ECC and REM models of Eqs. (4) and (6) respectively, and $\widetilde{\mathcal{H}_{mat}}$ the

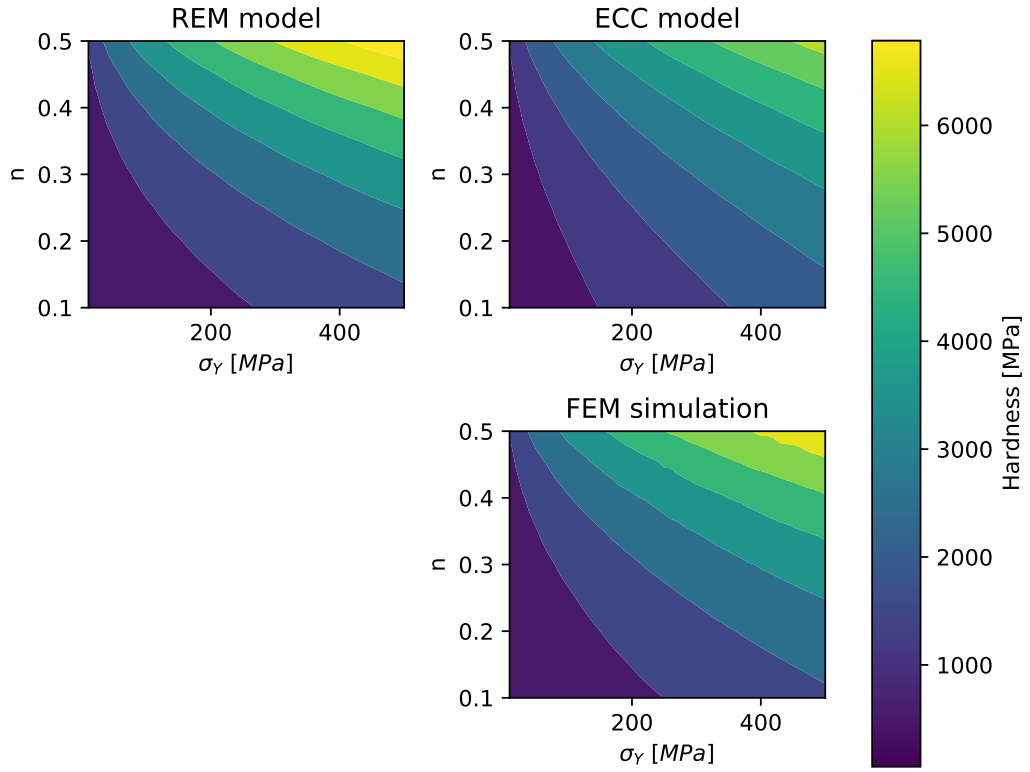

Figure 5: Maps of hardness values for REM, ECC models and FEM simulations, with $E = 210$ GPa and $\beta = 20°$

hardness obtained numerically by the FEM simulations

$$\epsilon = \frac{|\mathcal{H}_{mat} - \widetilde{\mathcal{H}_{mat}}|}{\widetilde{\mathcal{H}_{mat}}}. \tag{10}$$

Fig. 7 summarizes the main results obtained for $\beta = 20°$. Note the region highlighted in red that corresponds to hardening parameters typical of metallic sealing materials (copper, aluminium, nickel) with $0.2 \leqslant n \leqslant 0.3$ and $50\,\text{MPa} \leqslant \sigma_Y \leqslant 200\,\text{MPa}$. The ECC model yields very good results for a hardening exponent close to 0.3. The higher the yield stress, the higher the precision. However for the extreme case of low yield stress and low hardening exponent, the relative error can reach 50%. This corresponds to the asymptotic case of rigid perfectly plastic solids for which it is well known that expanding cavity based models fail (Johnson 1987). Unlike the ECC model, the REM model leads to errors lower than 10% over the whole investigated range of parameters. It is worth of interest to note that the REM model is almost insensitive to the yield stress. Its best accuracy is obtained in the range $0.2 \leqslant n \leqslant 0.3$, which corresponds to the range of sealing materials. For this latter case, the relative error is lower than 2.5%.

A wide range of angles is at stake in sealing surfaces so, in addition to $\beta = 20°$ (Fig. 7), Fig. 8 presents numerical results for angles $\beta = 15°$, 10° and 5°, focusing on the region of sealing materials.

Fig. 5 shows, for $\beta = 20°$, the evolution of hardness according to the studied parameters (σ_Y, n) of Hollomon's law. The analytical models have an evolution similar to FEM simulations especially the REM model. The hardness increases with the elastic limit and the hardening coefficient as expected by Cheng et al. 2004 The angle effect is shown on Fig. 6 for one material. The figure highlights that the two models error is function of the contact angle. Indeed, on the presented material, ECC is slightly more accurate than REM model for low angles (5°) while REM model is better for higher angles (15°). ~~With a smaller contact angle, REM model gradually under-performs but remains quite homogeneous with a relative error lower than 10%.~~ The REM model performs well for all studied angles with some privileged area according to strain hardening coefficient. Overall, its relative error stays lower than 10 %. The ECC model remains in good agreement near $n = 0.3$ as previously, but the corresponding zone becomes narrower. It is then outperformed by the REM model outside this thin and unpredictable area. ~~Finally, its heterogeneity is a problem in itself while the relative error of the REM model can be compared to a constant offset.~~

From these results it is thus recommended to use the REM model to compute the wedge hardness in the framework of sealing applications. However this model is restricted to single indentation (i.e., without interaction between the neighbouring asperities). To highlight this point, the hardness results obtained by FEM for the single indentation case are compared to those obtained for the case of multiple

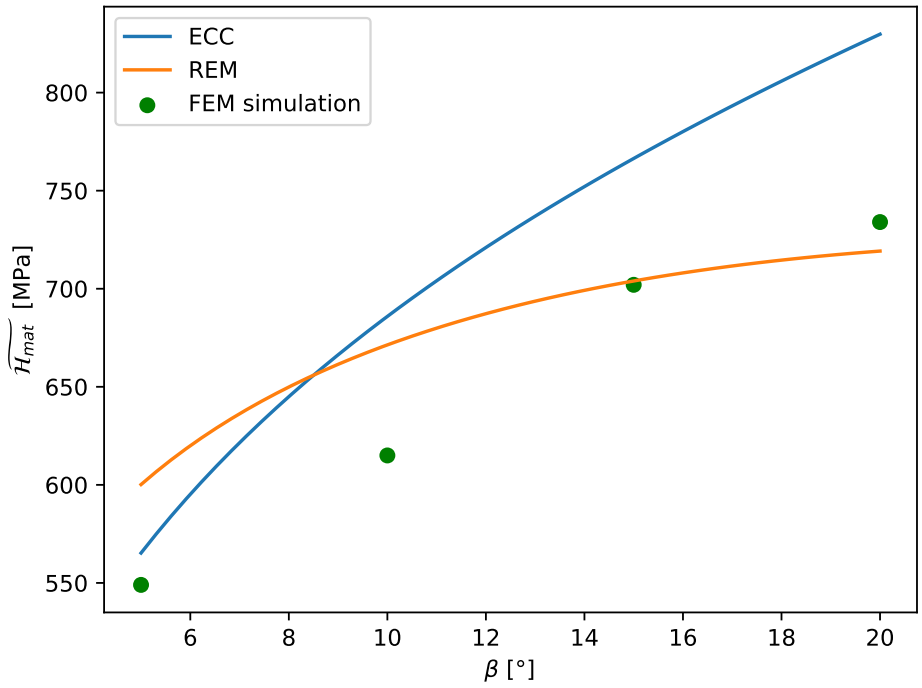

Figure 6: Hardness for all models and various contact angles for a material with $E = 210\,\text{GPa}$, $\sigma_Y = 102\,\text{MPa}$ and $n = 0.2$.

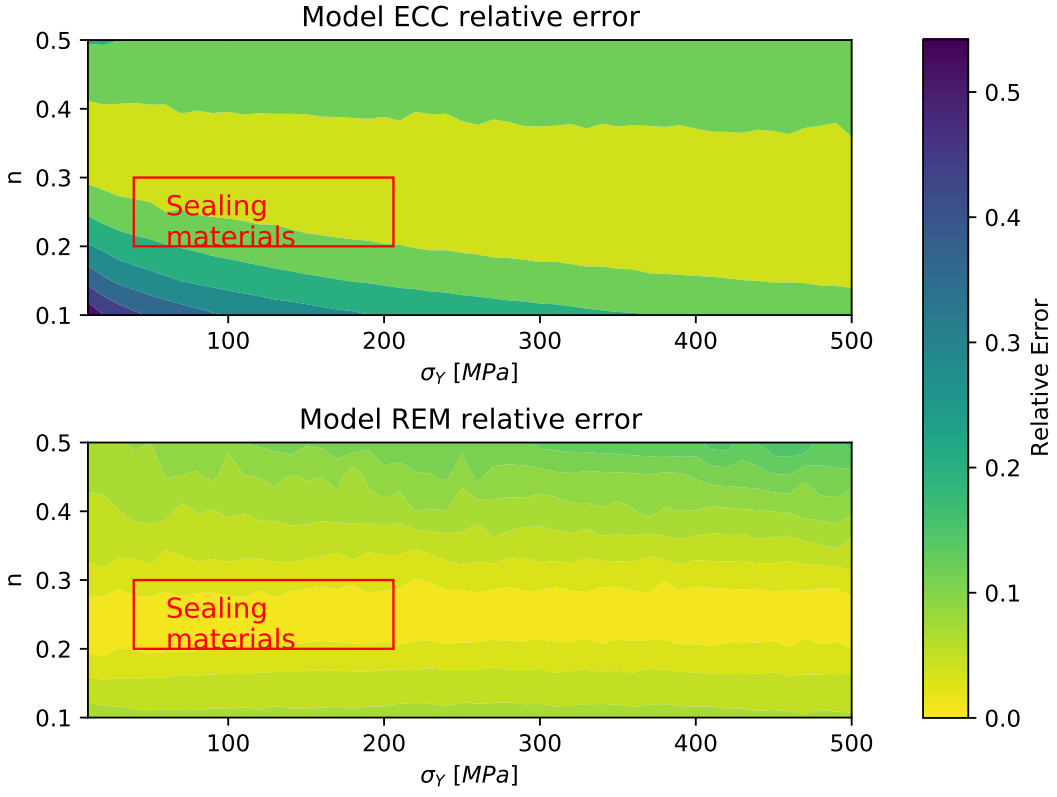

Figure 7: Error maps for single indentation models, with $E = 210\,\text{GPa}$ and $\beta = 20°$.

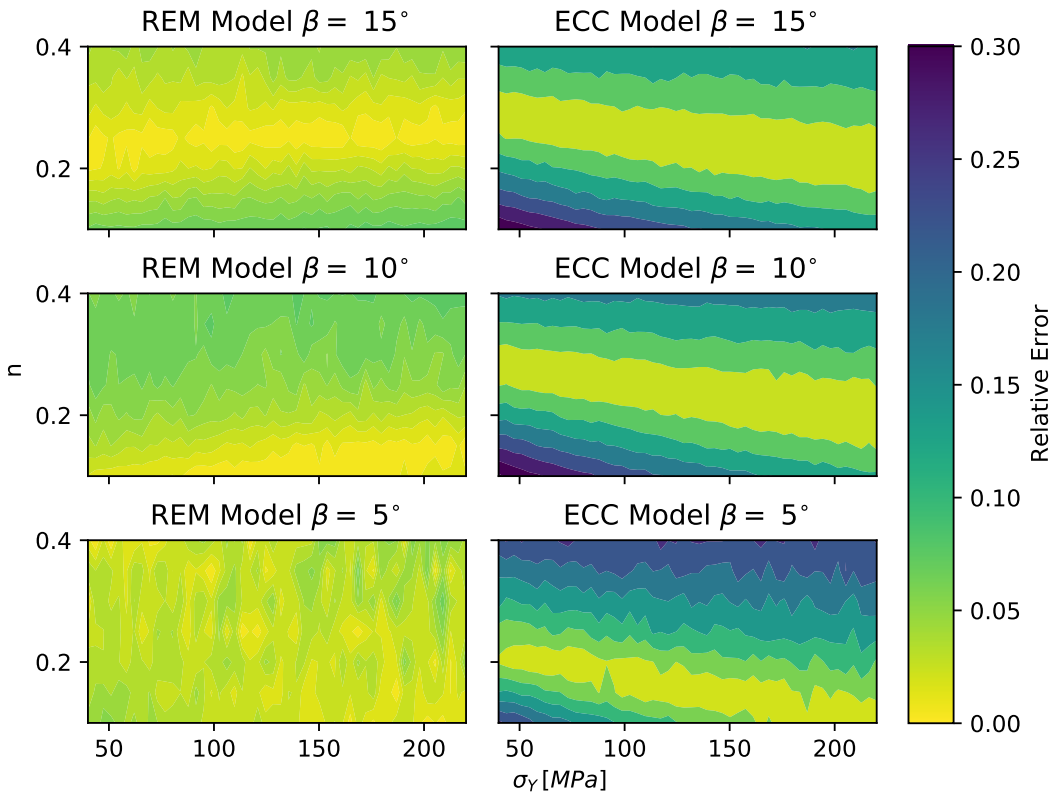

Figure 8: Error maps for single indentation models, with $\beta = 5°$, 10° and 15°.

wedges indentation as a continuous function of the applied load on the indenter. The evolution of the dimensionless apparent hardness $\mathcal{H}^* = \mathcal{H}/\mathcal{H}_{mat}$, is presented as a function of the applied indentation load in Fig. 9. As expected, the single indentation hardness does not depend upon load, while the multiple wedges indentation hardness increases quite rapidly with the load, indicating more and more prominent interaction effect between the indenters. Also, both model yield to the same result for the low load range (i.e., $\mathcal{H}^* \approx 1$). Results below a given load are not shown since the number of nodes in contact is not large enough. The increase at larger load is clearly the effect of tip interaction observed by Salikhyanov (2019). In other words, the single indentation stage is followed by the interaction stage that leads to an increase of mean contact pressure due to asperity interaction.

4.2 Multiple wedges indentation

Multiple indentation is observed through apparent hardness and dimensionless contact area. The results are presented using dimensionless quantities for a clarity purpose and to gain physical insight in the phenomena at play. First, the apparent hardness $\mathcal{H}$ is made dimensionless by the single wedge indentation

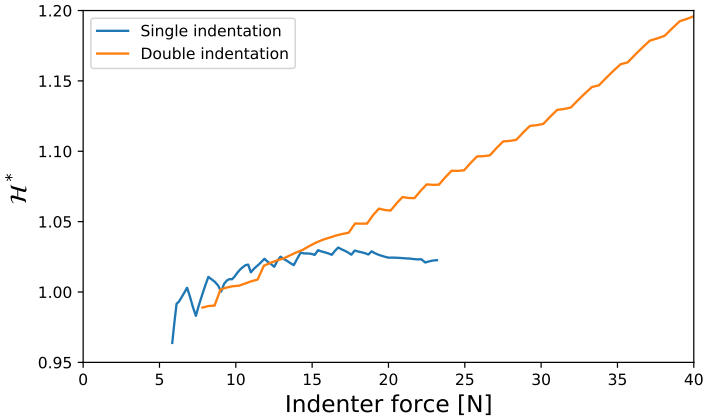

Figure 9: Comparison of the computed instantaneous hardness between single and multiple wedges indentation.

material hardness $\mathcal{H}_{mat}$ (computed using the REM model of Eq. (6)) as

$$\mathcal{H}^* = \frac{\mathcal{H}}{\mathcal{H}_{mat}}. \tag{11}$$

As observed in the previous section, such a dimensionless parameter will highlight the evolution of hardness due to interaction and hardening of the material. The dimensionless sealing force F^* is defined as

$$F^* = \frac{F}{W\mathcal{H}_{mat}}, \tag{12}$$

with F the actual force on the indenter and where $W\mathcal{H}_{mat}$ represents the force that would lead to full contact in a bearing contact model (Dapp et al. 2012), considering a constant mean pressure over the contact taken as the material hardness. In addition, note that we have the obvious relation $F^* = \mathcal{H}^* L^*$. The closing index $S^* = S/S_0$ is defined to monitor the evolution of the free space under the indenter with a scalar value. This gives an idea of the average gap between the indenter and the substrate, and hence of the sealing progress. In a similar manner, one can derive the dimensionless (projected) contact area L^* defined by

$$L^* = \frac{L_c}{W}, \tag{13}$$

L_c being the projected true contact length. The evolution of $\mathcal{H}^*$ as a function of the contact ratio L^* is shown in Fig. 10 to highlight the three main stages of sealing. This curve has been obtained considering the first geometry in Tab. 1 and Hollomon's parameters, $\sigma_Y = 100$ MPa and $n = 0.2$. The first stage is the single wedge indentation stage. As shown previously, the apparent hardness is well described by the wedge indentation REM model. The transition between the single indentation regime to the interaction regime is quite smooth. It is considered here that the interaction regime starts once the increase of the hardness is around 5%, that corresponds to a contact ratio $L^* \approx 0.25$. Within the interaction regime, the hardness seems to be proportional to the contact ratio. Once a given contact ratio of $L^* \approx 0.75$ is reached, the hardness starts increasing dramatically. This last regime is the global plastic locking regime that begins when the two neighbouring indentation-induced plastic flow fully recover. Contrary to slip line field calculations (Salikhyanov 2019), the sealing keeps increasing but at the cost of a fast increase of the apparent hardness. At full contact when $L^* \longrightarrow 1$, the hardness reaches a value close to 2.5 that of the single wedge indentation material hardness. The equivalent plastic strain field associated to each regime is given in Fig. 11, diamond markers in Fig. 10 specify the position of strain pictures on the $\mathcal{H}^*(L^*)$ curve. For the sake of illustration, it is possible to associate the plastic deformation (Fig. 11) to the slip-line fields hence following the expansion of both influence area and their interaction. This observation backs the point of a three steps closing with indenters interaction. However, simulations were made with elasto-plastic hardening materials while slip-line fields only stands for perfectly plastic materials so this comparison can not be further extended. Due to the boundary conditions and the isochoric plastic flow assumption, there is a volumetric change of elastic nature. It implies a rise in hydrostatic pressure, which in turns leads to a rise of contact pressure. This rise is really significant for the last stage of sealing. The hydrostatic pressure is also a consequence of indenter interactions. Note that theses results have been obtained for a given configuration In the two following sections, effects of indenter geometry and strain hardening parameters will be investigated in details.

4.2.1 Effects of the geometrical parameters

Fig. 12 presents the evolution of $\mathcal{H}^*$, F^* and S^* as a function of L^* for the five multiple wedges indentation geometries defined in Tab. 1. The strain hardening parameters remain the same for each calculation, their values were chosen as $\sigma_Y = 100$ MPa and $n = 0.2$. The three sealing stages are clearly visible. $\mathcal{H}^*$ and S^* seems to be geometry-independent. Despite a difference of material behaviour, theoretical investigation of Hill (1950) in perfect plasticity and Johnson (1987); Sneddon (1995) in perfect elasticity let us expect a dependence on bulk height B which is not confirmed by our results. It might however not be excluded that L^* and S^* already include somehow the influence of the height. Therefore it is recommended to not consider B as a driving parameter for the interaction stage of sealing. The only geometrical parameter which seems worth of interest is the contact angle β. The difference between 10° and 5° is however not important enough to be clearly visible on Fig. 12. Note that Fig. 12-c points out the closing kinetic during multiple wedges indentation. The bearing contact model is a purely geometrical model based on the concept of erosion (Dapp et al. 2012). The indenter displacement consumes material on its way without provoking any elastic or plastic deformations. A contact pressure is associated to this contact and corresponds to the hardness of the eroded material $\mathcal{H}_{mat}$. The response of this model to multiple wedges indentation is drawn in dashed lines on Fig. 12. It further shows the differences brought by interaction of indenters. These results show that sealing regimes can be described through dimensionless parameters that are almost geometry-independent.

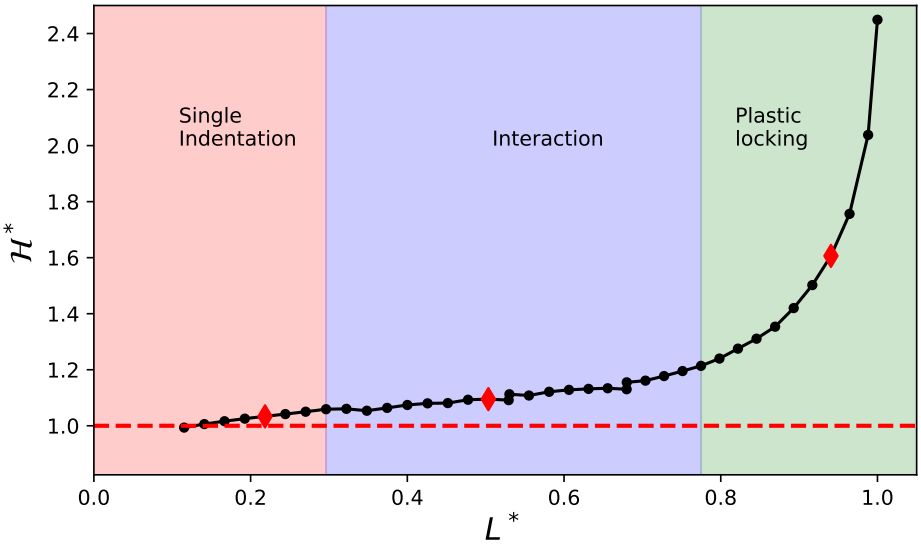

Figure 10: Typical evolution of the hardness as a function of the contact width in multiple wedges indentation, highlighting the three steps with diamond markers for Fig. 11 fields.

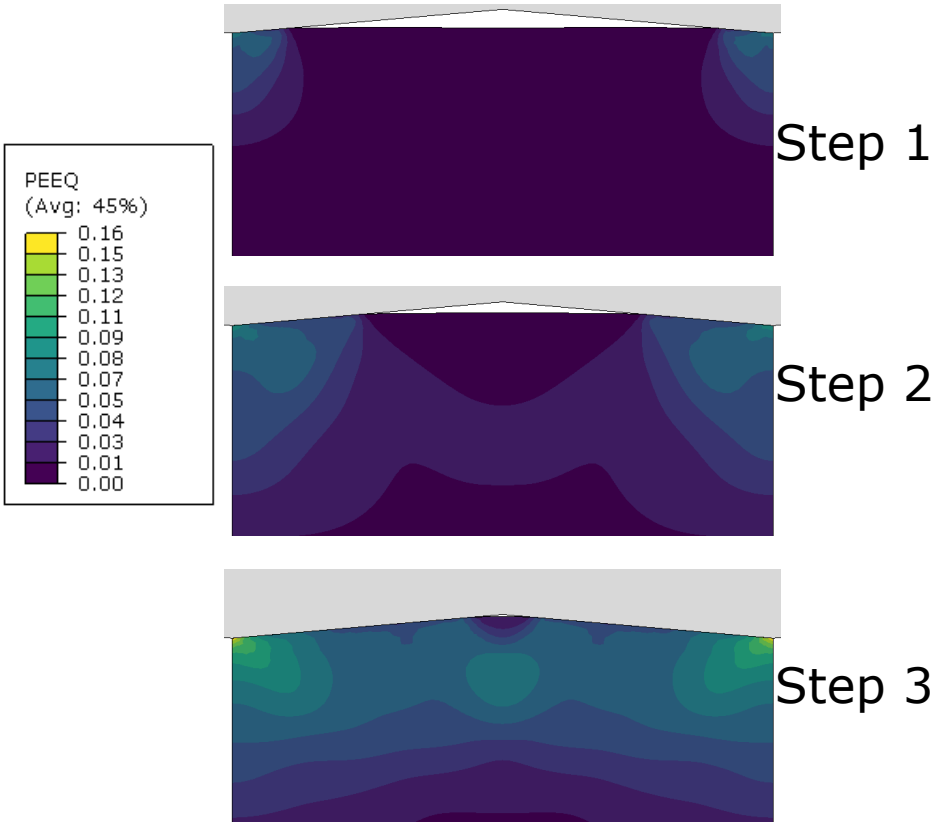

Figure 11: Field of the equivalent plastic strain computed in ABAQUS® for the three stages of the multiple wedges indentation.

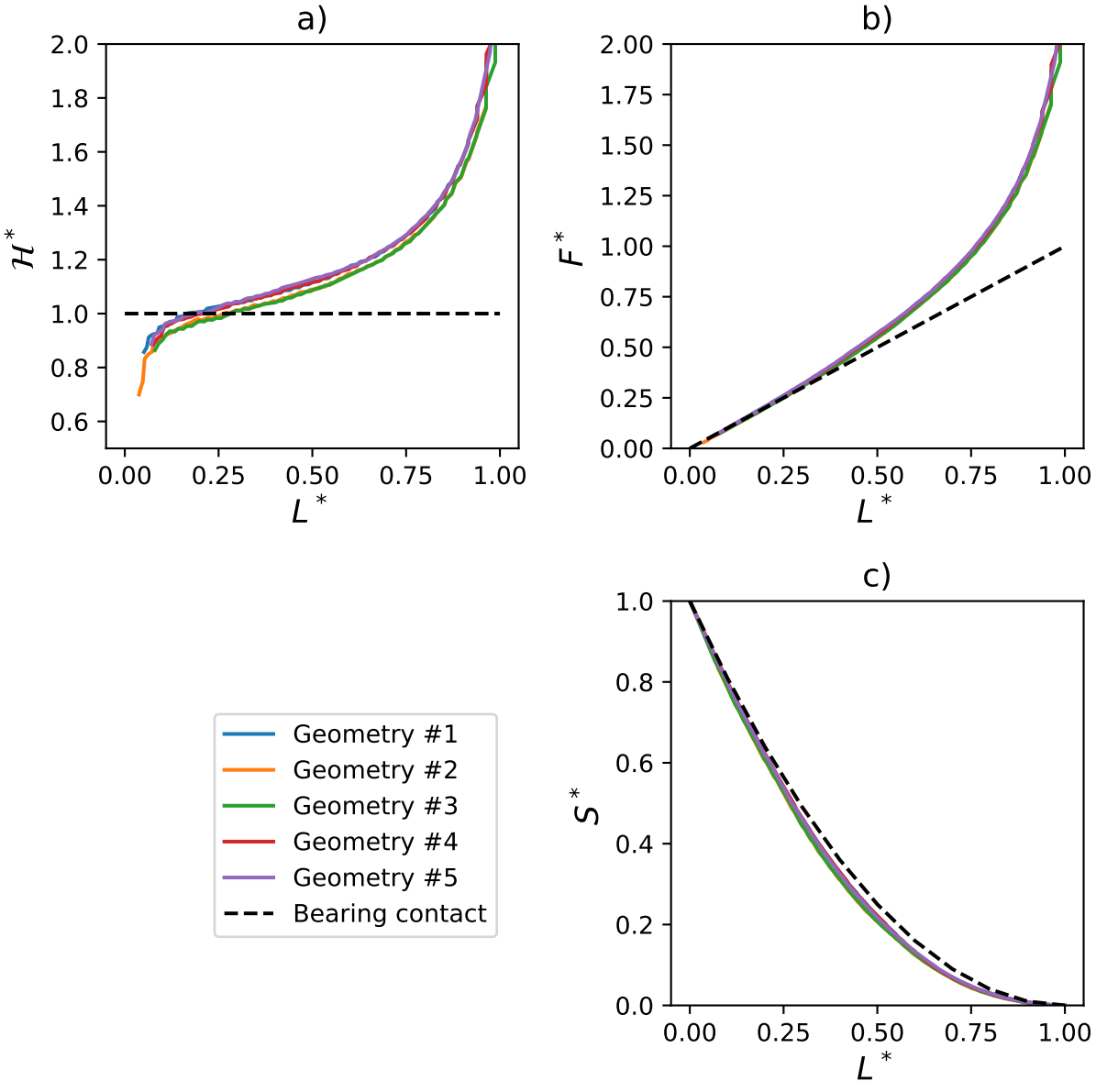

Figure 12: Influence of the geometrical parameters (see Tab. 1) on multiple wedges indentation. The results from the bearing contact model are given as dashed lines.

4.2.2 Effects of the material parameters

Let us now vary the strain hardening parameters and fix the geometrical configuration to $\beta = 10°$, $W = 0.1$ mm and $B = 1$ mm (corresponding to geometry #1 in Tab. 1). The influence of the yield stress is presented in Fig. 13. As expected from Eq. (1) the normalization by $\mathcal{H}_{mat}$ totally transfers the effect of σ_Y to the single indentation step. Moreover further steps do not seem to be modified by a variation in the yield stress. The kinetic of closing in Fig. 13-c is not significantly influenced by σ_Y and is quite similar to the simple bearing contact in this case, it argues for few sink-in or pile-up behaviour in these material and geometrical conditions.

Fig. 14-a shows the effects of the strain hardening exponent n on the evolution of $\mathcal{H}^*$ as a function of L^*. Note that here again, the three sealing stages are still clearly observable. The strain hardening parameter n seems to have a significant influence on both the slope of the interaction stage and the start of the plastic locking stage. The higher the strain hardening exponent, the faster the hardness increase. However, this is particularly visible for larger contact ratio. Let us note that $\mathcal{H}^*$ is not equal to 1 for $n = 0.4$ at low contact ratio and the expected plateau-like evolution of single wedge indentation is not visible. This may be a consequence of the REM hardness model which may lead to some error for such value of the strain hardening exponent. It can also be a consequence of a smaller single indentation regime when the strain hardening parameter increases. The finite element mesh might be too coarse to catch this regime properly as well. For sealing like material ($n \approx 0.2$), the plateau-like regime is clearly visible. It is followed as expected by a linear, then by a fast increase of the hardness. It is therefore clearly observed here that the asperities interaction effect is enhanced by the strain hardening ability of sealing materials. As a matter of fact, it would be better to use materials exhibiting a low strain hardening exponent for sealing applications. Let us note that this significant effect of n prevents the use of the theoretical frameworks of Hill et al. (1947) or Salikhyanov (2019) to quantitatively predict the sealing process.

The evolution of the closing index is also affected by the strain hardening ability of the sealing material as shown in Fig. 14-c. At first, it may be surprising to state that the highest impact is observed during the single indentation and interaction stages and not the plastic locking stage. Let us remember that the closing index is only related to the shape of the free surface for a given contact ratio. Therefore piling up and sinking ability of the material will play a significant role. It is well known from single indentation theory that a low strain hardening exponent n will lead to the rise up of a ridge whereas a high strain hardening exponent will prevent the formation of this ridge (Cheng et al. 2004). This is illustrated in Fig. 16.

For $n = 0.3$ (consequentially $n = 0.4$), a sink-in is observed in single indentation as shown in Fig. 15. For multiple wedges indentation, sink-in and pile-up are more difficult to detect. Indeed, the contact depth over penetration depth ratio h_c/h is badly defined in this case. Moreover, some additional factors can be involved in this behaviour with for example the plastic flow of the material confined by the groove formed by the two neighbouring indenters. It makes the comparison difficult with the classical comprehension of the pile-up or sink-in as presented in Bolshakov et al. 1998; Cheng et al. 2004, since more parameters are at stake. Therefore we can ascertain that the higher the strain hardening parameter n, the lower the closing index for a given contact ratio but it cannot be entirely linked to pile-up (or sink-in) behaviour. Within the plastic locking stage, the materials generally flows up homogeneously to fill the remaining free volume for symmetric indenter angles. In Fig. 12, 13 and 14, the black dashed line stands for the bearing contact model. This model is quite satisfying to describe the closing index, especially for low hardening, but performs poorly when it comes to the prediction of the force (or hardness), especially at the end of the interaction step and the plastic locking step. This means that the present simulations can help correct and predict the necessary force for sealing while the geometrical kinetics of sealing is more difficult to understand through them and rather be described by a simpler model as the bearing contact one. ~~Therefore the higher the strain hardening parameter n, the lower the closing index for a given contact ratio. As discussed before the plastic locking stage starts when the two neighboring indentation-induced plastic strain field recover each other. Within this regime there is no more indentation pile-up and the materials flow up homogeneously to fill up the remaining free volume. This is the reason why the evolution of the closing index S^* as a function of the contact ratio L^* is no more dependent on the strain hardening exponent. Eventually, the start of the plastic locking regime might be determined from such a plot by measuring the minimum value of the contact ratio for which the curves merge into a single curve.~~

Interestingly, the dimensionless sealing force F^* presented in Fig. 14-b is only slightly affected by the strain hardening exponent up to the start of the plastic locking stage. The dimensionless sealing force F^* corresponds to the elementary force acting over two neighboring asperities. It is thus prone to be used in a reduced model (Yastrebov et al. 2011) aiming at predicting the sealing ability of surfaces based on arrays of wedge, typical of face-turned surface.

The present study aims at understanding how sealing materials can flow up to achieve a full contact between a rigid rough surfaces and a soft material. To this end, a dry contact was considered, that is no fluid is present and could be entrapped at the interface, especially in closed cavities resulting from

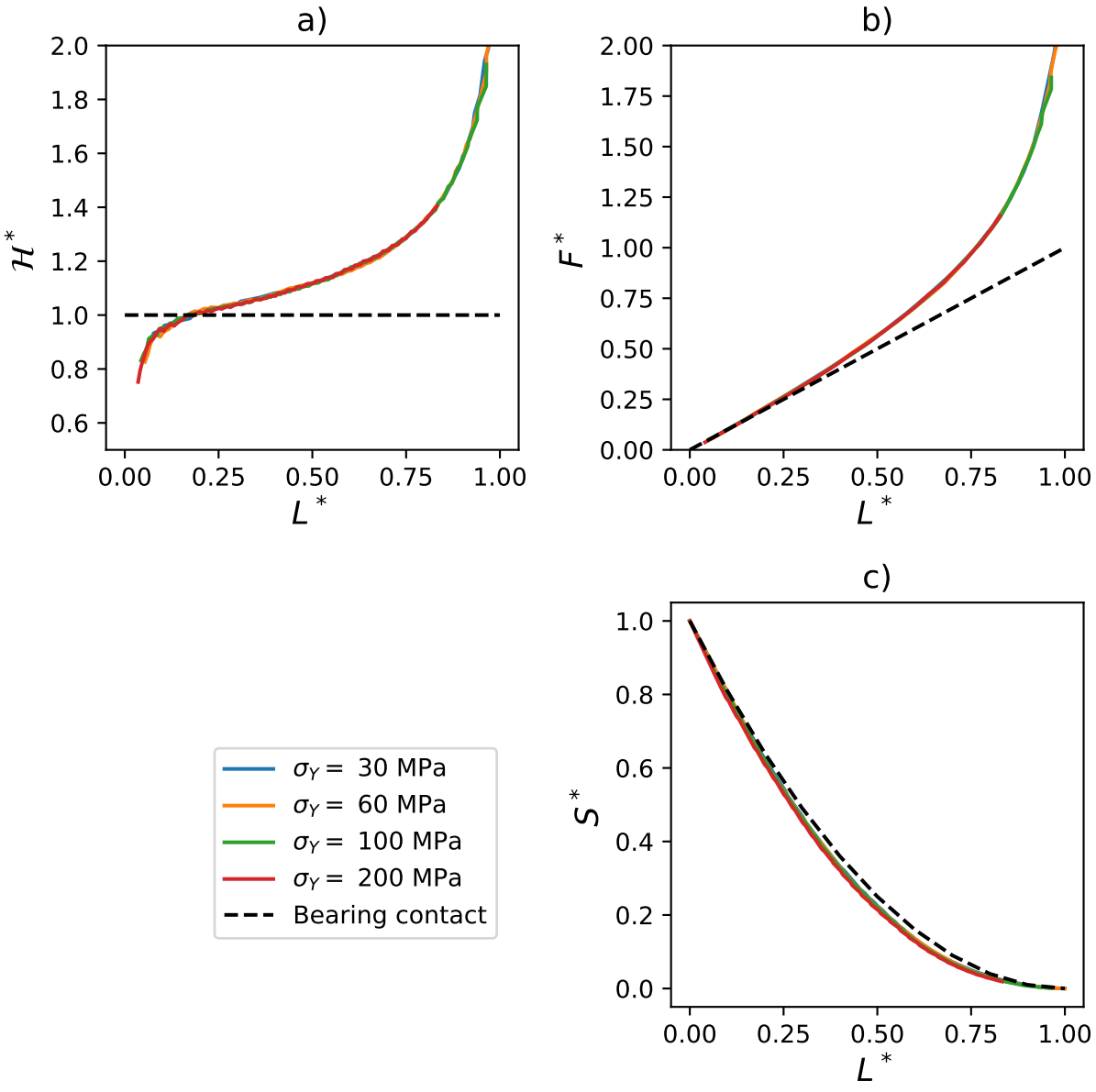

Figure 13: Influence of the yield stress on the multiple wedges indentation, with $n = 0.2$.

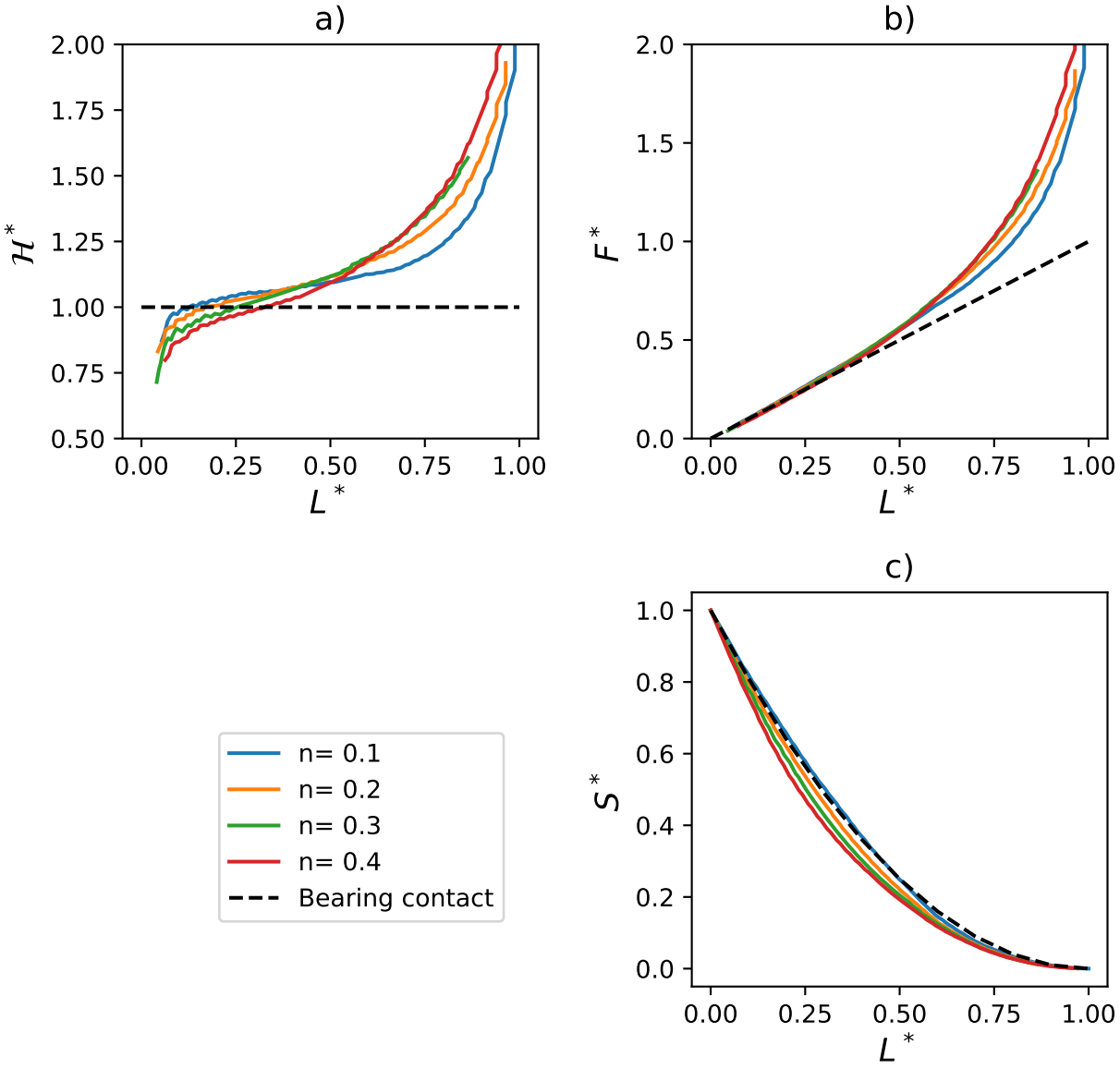

Figure 14: Influence of the strain hardening exponent n on multiple wedges indentation, with $\sigma_Y = 100\,\text{MPa}$.

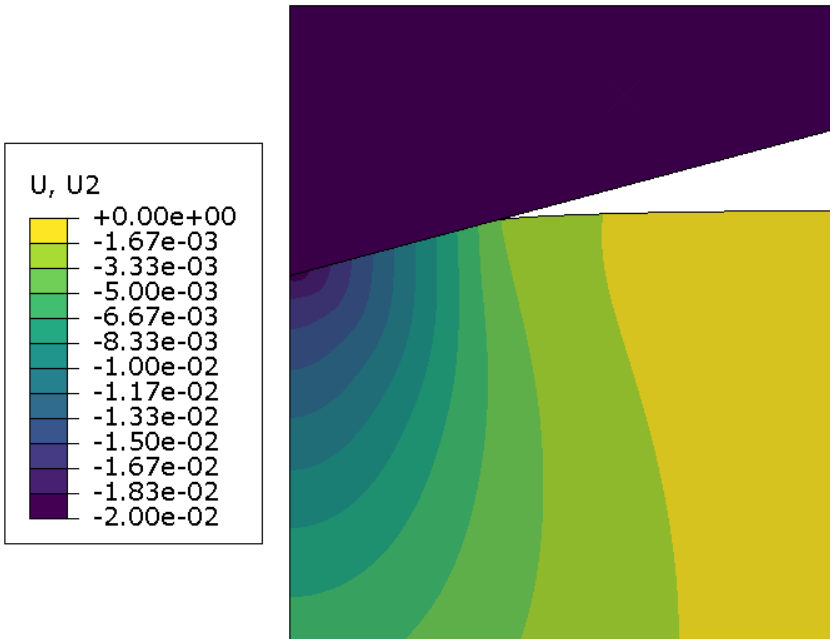

Figure 15: Computed vertical displacement field in single indentation (with $n = 0.3$). Sink-in is observed as the displacement is negative.

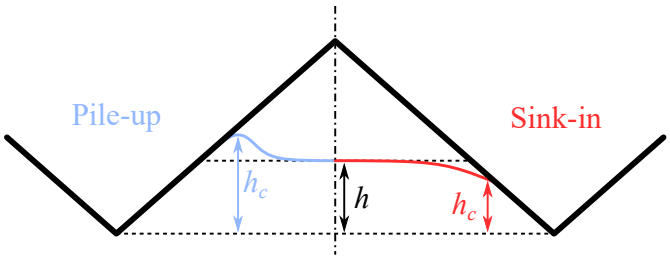

Figure 16: Illustration of the pile-up (blue) and sink-in (red) behaviours of the deformed surface in indentation.

surrounding surface deformation during the indentation process. The usage of this framework is mainly motivated by the fact that metal seals are generally installed and compressed under dry conditions in practice. However, when a fluid is present at the interface, the problem obviously becomes more complicated as simulations accounting for fluid-solid interactions are required to describe such behaviour (Azushima et al. 1995; Bech et al. 1999). In this case, it might be assumed that the three stages would be greatly modified. Indeed, an entrapped fluid would bear a part of the load actually decreasing contact pressure on the material surface and eventually decreasing the resulting contact area. Shvarts et al. 2018 however consider that for realistic fluids and material no dramatic opening of the contact takes place. To extend the use of our work to wet surfaces as such found in lubrication problem, it would thus be necessary to run additional simulations with entrapped fluid.

5 Conclusions

This article dealt with wedge indentation in the framework of sealing. The objective was to investigate with the help of the finite element method how the mean contact pressure increases when two wedge indenters interact up to the full closing of the cavity in-between. Three successive indentation regimes are clearly evidenced. The first regime is the single wedge indentation one and is characterized by a constant mean pressure called material hardness. When approximately 25% of the total projected area is in contact, the second regime begins. It is defined as the interaction one and corresponds to a linear increase of the mean contact pressure as a function of the contact length. The third and last regime takes place after 75% of contact and is the plastic locking regime defined by a fast pace increase in contact pressure up to full closing. The results are rather consistent with slip lines field theory (Salikhyanov 2019). Note that this theory is restrictive since it is limited to rigid perfectly plastic solids. We should also recall that the law used in our simulation does not describe well high deformation behaviour so flat value of apparent hardness at high contact ratio is not accurate. An experimental verification would be of great interest to measure the resulting error. Nevertheless, although this paper appears as a first step in this very complex field, some first conclusions of interest can be drawn for the indentation and sealing communities:

- *Single indentation regime*
  - For contact angle of 20° and within the range of metallic materials for sealing, the hardness is modelled with an accuracy of 2.5% using the Representative Elastic Material model developed by Kermouche et al. (2005).
  - The adaptation of the Gao et al. (2006) expanding cavity model to wedge indentation leads also to satisfactory results, with a lesser accuracy regarding sealing materials nonetheless.
- *Interaction regime*
  - The use of suitable dimensionless quantities leads us to show that the interaction regime is almost geometry-independent, which is of primary importance regarding the development of further reduced sealing contact models.
  - The main parameter governing the interaction regime is the strain hardening exponent. A higher strain hardening exponent leads to the start of the interaction regime for a lower contact length and a higher increase of the hardness.
- *Plastic locking regime*
  - Contrary to slip line field prediction, the plastic locking regime is not really “locked”. The sealing can proceed up to full closing, at the cost however of a fast increase of the apparent hardness, up to two to three times the single wedge indentation hardness. It fixes a virtual limit for closing, hence sealing, to approximately 80% of total projected area.
  - Here again, the main parameter governing the interaction regime is the strain hardening exponent n. A higher strain hardening exponent leads to the start of the plastic regime for a lower contact length and a higher increase of the hardness.
- *About sealing*
  - For a given hardness, the best sealing materials are those that can delay the start of the interaction regime, that is those with the lowest strain hardening exponent n.
  - The sealing of face-turned surface can be complete only once the plastic locking regime is ended for one groove.

Acknowledgements

The authors are grateful to the CEA and Technetics Group France for funding this research through the joint *Maestral* sealing laboratory.

References

Azushima, A. and H. Kudo (1995). "Direct observation of contact behaviour to interpret the pressure dependence of the coefficient of friction in sheet metal forming". *CIRP annals* 44.1, pp. 209–212. DOI: https://doi.org/10.1016/S0007-8506(07)62309-9. URL: https://www.sciencedirect.com/science/article/pii/S0007850607623099

Bech, J., N. Bay, and M. Eriksen (1999). "Entrapment and escape of liquid lubricant in metal forming". *Wear* 232.2, pp. 134–139. DOI: https://doi.org/10.1016/S0043-1648(99)00136-2. URL: https://www.sciencedirect.com/science/article/pii/S0043164899001362

Bolshakov, A. P. G. M. and G. M. Pharr (1998). "Influences of pileup on the measurement of mechanical properties by load and depth sensing indentation techniques". *Journal of materials research* 13.4, pp. 1049–1058

Cheng, Y.-T. and C.-M. Cheng (2004). "Scaling, dimensional analysis, and indentation measurements". *Materials Science and Engineering: R: Reports* 44.4-5, pp. 91–149. DOI: 10.1016/j.mser.2004.05.001. URL: https://linkinghub.elsevier.com/retrieve/pii/S0927796X04000415

Dapp, W. B., A. Lücke, B. N. J. Persson, and M. H. Müser (2012). "Self-affine elastic contacts: percolation and leakage". *Physical Review Letters* 108.24, p. 244301. DOI: 10.1103/PhysRevLett.108.244301. URL: https://link.aps.org/doi/10.1103/PhysRevLett.108.244301

Dumas, M., D. Fabre, F. Valiorgue, G. Kermouche, A. Van Robaeys, M. Girinon, A. Brosse, H. Karaouni, and J. Rech (2021). "3D numerical modelling of turning-induced residual stresses – A two-scale approach based on equivalent thermo-mechanical loadings". *Journal of Materials Processing Technology* 297, p. 117274. DOI: https://doi.org/10.1016/j.jmatprotec.2021.117274. URL: https://www.sciencedirect.com/science/article/pii/S092401362100234X

Feng, G., S. Qu, Y. Huang, and W. D. Nix (2007). "An analytical expression for the stress field around an elastoplastic indentation/contact". *Acta Materialia* 55.9, pp. 2929–2938. DOI: https://doi.org/10.1016/j.actamat.2006.12.030. URL: https://www.sciencedirect.com/science/article/pii/S1359645407000481

Gao, X.-L. (2003). "Elasto-plastic analysis of an internally pressurized thick-walled cylinder using a strain gradient plasticity theory". *International Journal of Solids and Structures* 40.23, pp. 6445–6455. DOI: 10.1016/S0020-7683(03)00424-4. URL: http://www.sciencedirect.com/science/article/pii/S0020768303004244

Gao, X.-L., X. N. Jing, and G. Subhash (2006). "Two new expanding cavity models for indentation deformations of elastic strain-hardening materials". *International Journal of Solids and Structures* 43.7, pp. 2193–2208. DOI: 10.1016/j.ijsolstr.2005.03.062. URL: http://www.sciencedirect.com/science/article/pii/S0020768305001836

Hill, R. (1950a). "LXVII. A theoretical investigation of the effect of specimen size in the measurement of hardness". *The London, Edinburgh, and Dublin Philosophical Magazine and Journal of Science* 41.319, pp. 745–753. DOI: 10.1080/14786445008561007. URL: https://doi.org/10.1080/14786445008561007

Hill, R. (1950b). *The mathematical theory of plasticity*. Clarendon Press

Hill, R., E. H. Lee, S. J. Tupper, and N. F. Mott (1947). "The theory of wedge indentation of ductile materials". *Proceedings of the Royal Society of London. Series A. Mathematical and Physical Sciences* 188.1013, pp. 273–289. DOI: 10.1098/rspa.1947.0009. URL: https://royalsocietypublishing.org/doi/abs/10.1098/rspa.1947.0009

Johnson, K. L. (1970). "The correlation of indentation experiments". *Journal of the Mechanics and Physics of Solids* 18.2, pp. 115–126. DOI: https://doi.org/10.1016/0022-5096(70)90029-3. URL: https://www.sciencedirect.com/science/article/pii/0022509670900293

Johnson, K. L. (1987). *Contact mechanics*. Cambridge University Press

Kermouche, G., J.-L. Loubet, and J.-M. Bergheau (2005). "An approximate solution to the problem of cone or wedge indentation of elastoplastic solids". *Comptes Rendus Mécanique* 333.5, pp. 389–395. DOI: 10.1016/j.crme.2005.04.001. URL: https://linkinghub.elsevier.com/retrieve/pii/S1631072105000689

Meguid, S. A., I. F. Collins, and W. Johnson (1977). "The co-indentation of a layer by two flat plane or spherical-headed, rigid punches". *International Journal of Mechanical Sciences* 19.1, pp. 1–9. DOI: 10.1016/0020-7403(77)90010-8. URL: https://linkinghub.elsevier.com/retrieve/pii/0020740377900108

Meguid, S. A. and M. S. Klair (1985). "Elasto-plastic co-indentation analysis of a bounded solid using finite element method". *International Journal of Mechanical Sciences* 27.3, pp. 157–168. DOI: 10.1016/0020-7403(85)90056-6. URL: https://linkinghub.elsevier.com/retrieve/pii/0020740385900566

Oliver, W. C. and G. M. Pharr (1992). "An improved technique for determining hardness and elastic modulus using load and displacement sensing indentation experiments". *Journal of Materials Research* 7.6, pp. 1564–1583. DOI: 10.1557/JMR.1992.1564

Pérez-Ràfols, F., R. Larsson, and A. Almqvist (2016). "Modelling of leakage on metal-to-metal seals". *Tribology International* 94, pp. 421–427. DOI: 10.1016/j.triboint.2015.10.003. URL: http://www.sciencedirect.com/science/article/pii/S0301679X15004521

Poon, B., D. Rittel, and G. Ravichandran (2008). "An analysis of nanoindentation in elasto-plastic solids". *International Journal of Solids and Structures* 45.25-26, pp. 6399–6415. DOI: https://doi.org/10.1016/j.ijsolstr.2008.08.016. URL: https://www.sciencedirect.com/science/article/pii/S0020768308003259

Robbe-Valloire, F. and M. Prat (2008). "A model for face-turned surface microgeometry: Application to the analysis of metallic static seals". *Wear* 264.11-12, pp. 980–989. DOI: 10.1016/j.wear.2007.08.001. URL: http://www.sciencedirect.com/science/article/pii/S0043164807005923

Salikhyanov, D. (2019). "Contact mechanism between dissimilar materials under plastic deformation". *Comptes Rendus Mécanique* 347.8, pp. 588–600. DOI: 10.1016/j.crme.2019.07.002. URL: https://linkinghub.elsevier.com/retrieve/pii/S1631072119301214

Shvarts, A. G. and V. A. Yastrebov (2018). "Trapped fluid in contact interface". *Journal of the Mechanics and Physics of Solids* 119, pp. 140–162. DOI: https://doi.org/10.1016/j.jmps.2018.06.016. URL: https://www.sciencedirect.com/science/article/pii/S0022509617311031

Sneddon, I. N. (1965). "The relation between load and penetration in the axisymmetric Boussinesq problem for a punch of arbitrary profile". *International Journal of Engineering Science* 3.1, pp. 47–57. DOI: https://doi.org/10.1016/0020-7225(65)90019-4. URL: https://www.sciencedirect.com/science/article/pii/0020722565900194

Sneddon, I. N. (1995). *Fourier transforms*. Dover Publications

Studman, C. J., M. A. Moore, and S. E. Jones (1977). "On the correlation of indentation experiments". *Journal of Physics D: Applied Physics* 10.6, pp. 949–956. DOI: 10.1088/0022-3727/10/6/019. URL: https://doi.org/10.1088/0022-3727/10/6/019

Tabor, D. (1951). *The hardness of metals*. Oxford University Press

Tabor, D. (1996). "Indentation hardness: Fifty years on a personal view". *Philosophical Magazine A* 74.5, pp. 1207–1212. DOI: 10.1080/01418619608239720. URL: http://www.tandfonline.com/doi/abs/10.1080/01418619608239720

Yastrebov, V. A., J. Durand, H. Proudhon, and G. Cailletaud (2011). "Rough surface contact analysis by means of the Finite Element Method and of a new reduced model". *Comptes Rendus Mécanique* 339.7-8, pp. 473–490. DOI: 10.1016/j.crme.2011.05.006. URL: https://linkinghub.elsevier.com/retrieve/pii/S163107211100091X

A Mesh convergence study – single wedge indentation

The physical quantity studied by the single wedge indentation simulation is the contact pressure under the tip of the indenter (i.e. the hardness). It is computed by dividing the vertical indentation force by the projected contact area for multiple penetrations. The average value over these penetrations is kept to limit mesh effects, and this is valid since the stress and strain fields are supposed to be geometrically similar. To assess the effect of mesh refinement on the computed hardness, the following error is defined

$$\epsilon = \frac{|\mathcal{H}_{mesh} - \mathcal{H}_{ref}|}{\mathcal{H}_{ref}}, \tag{14}$$

where $\mathcal{H}_{mesh}$ is the hardness computed for a given mesh size and $\mathcal{H}_{ref}$ is the reference hardness, chosen as that obtained for the finest mesh. Fig. 17 presents the evolution of this error for various meshes and materials. The mesh size is expressed in terms of elements at the surface of the contact area. These elements are responsible for the measure of contact area and contact pressure and, as such, should be numerous to described the contact properly. It can be observed that even for a coarse mesh, the error made is less than 0.6%, with few improvement when elements are doubled from 120 (0.8% ratio) to 240 (0.4% ratio). We thus conclude that the mesh is converged and that even for comparatively coarse mesh the effect is weak. In the present study of single wedge indentation, 65 elements (1.5% ratio) in the contact area are utilized.

B Mesh convergence study – multiple wedges indentation

For the multiple wedges indentation, we define the following error over the entire indentation regime

$$\epsilon = \frac{\int |\mathcal{H}^*_{mesh} - \mathcal{H}^*_{ref}| \, \mathrm{d}L^*}{\int \mathcal{H}^*_{ref} \, \mathrm{d}L^*}, \tag{15}$$

where again $\mathcal{H}^*_{mesh}$ is the dimensionless hardness for a given mesh size, $\mathcal{H}^*_{ref}$ is a reference dimensionless hardness (that obtained with the most refined mesh) and L^* is the dimensionless contact length. Fig. 18 shows the evolution of the error as a function of the relative mesh size (ratio of the element size and the distance between the indenters W). The error is relatively small even for coarse meshes. However, the mesh produces an oscillation-like effect due to the discrete variation of the contact length (see Fig. 19). This local discrete variation is quite misleading so the focus of the present study should be laid upon a locally average variation of the quantities instead. To this end, a sliding average filter is employed so as to use a relatively coarse mesh while having a reasonable computational time. The effects of using such

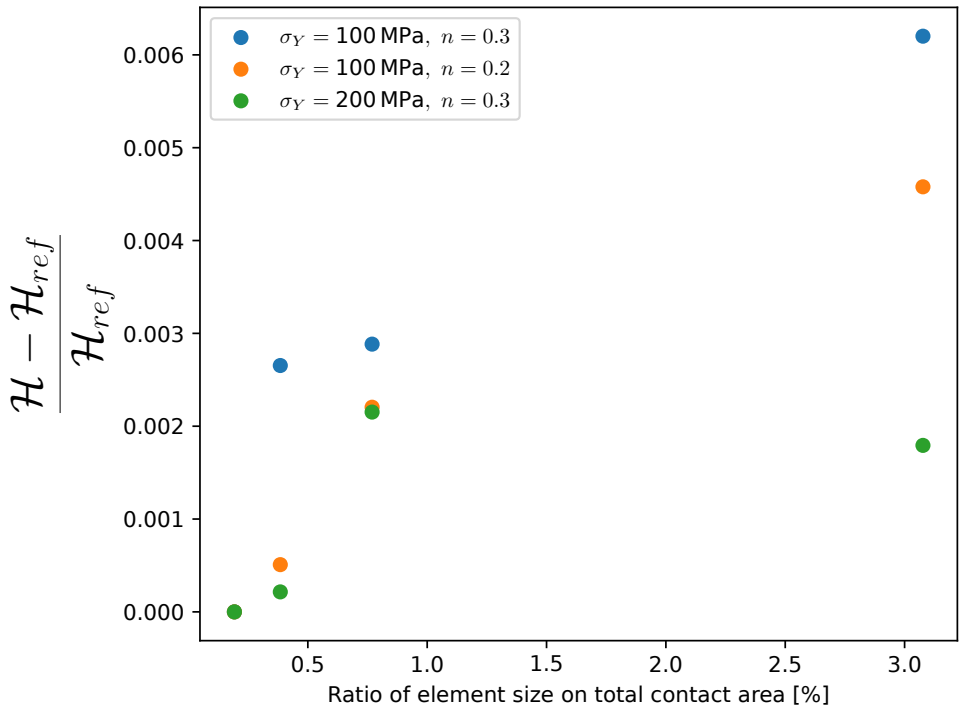

Figure 17: Evolution of the error on the single indentation hardness as a function of the relative mesh size, using the most refined mesh as reference.

sliding average filters are shown in Fig. 20. The hardness for the coarse meshes is then in better agreement with that obtained with the more refined ones. Nevertheless, the averaging window acts severely on the first points which were presenting the widest oscillation, and the average value falls below the ratio $\mathcal{H}^* = 1$ at small contact length. Note that this effect is mostly resolved from $L^* = 0.2$ onward, that is the interval of interest of the current study. The mesh convergence holds for several materials and it can be concluded that the dependencies of the apparent hardness on the hardening coefficient or yield stress observed in this article are not due to a mesh effect. In this article, a mesh ratio of 1% relative to the distance W between indenters is kept.

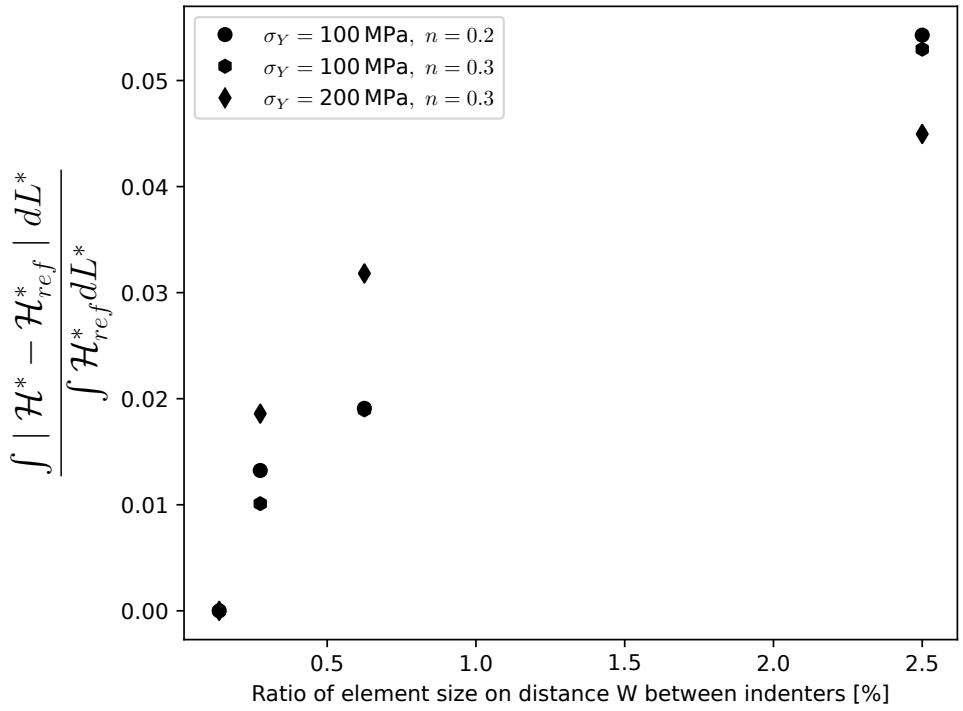

Figure 18: Evolution of the error on the multiple wedges indentation hardness as a function of the relative mesh size, using the most refined mesh as reference.

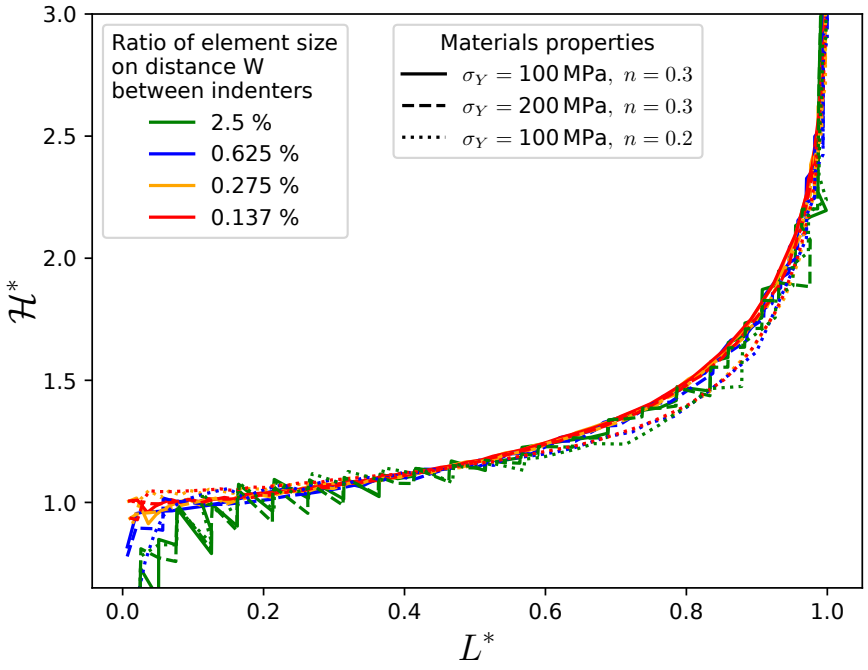

Figure 19: Apparent hardness as a function of the normalized contact area for different mesh size and different materials without averaging filter

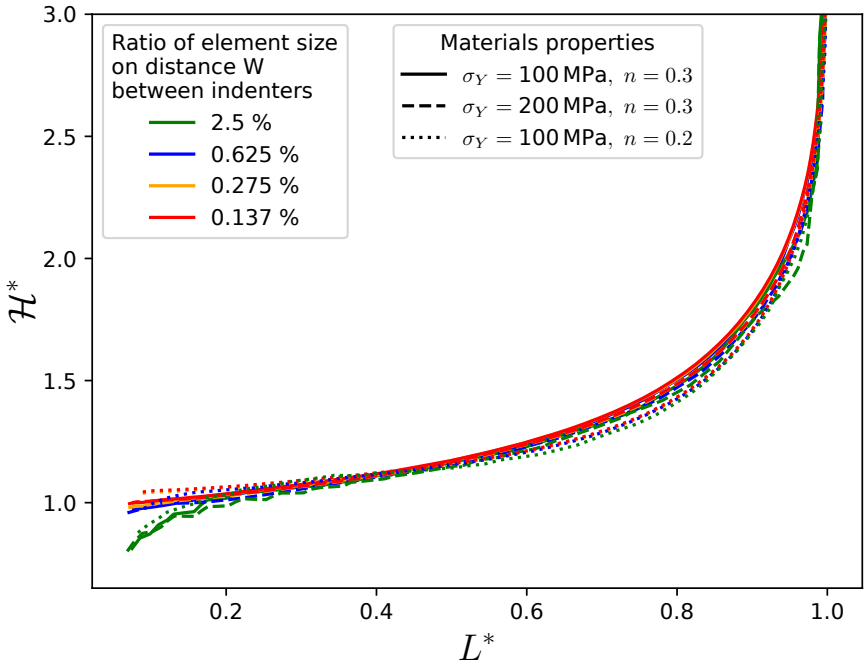

Figure 20: Apparent hardness as a function of the normalized contact area for different mesh size and different materials using an averaging filter